ARMA 25–0361

Insights into the hydro-mechanical behavior of a decimeter-scale fracture using the mini-SIMFIP probe

Osten, J., Jalali, M.R., Amann, F.
Chair of Engineering Geology and Hydrogeology, RWTH Aachen, Aachen, Germany
Cadmus, A
Chair of Geotechnical Engineering and Institute of Geomechanics and Underground Technology, RWTH Aachen, Aachen, Germany
Cook, P.J. and Guglielmi, Y.
Lawrence Berkeley National Laboratory, Berkeley, CA, USA

ABSTRACT: Understanding hydro-mechanical couplings in fractured rocks is essential for predicting the rock mass response during high-pressure fluid injection, including the stimulation of enhanced geothermal systems. However, fluid-driven fracture dislocations are challenging to measure due to the need for local displacement data at high fluid pressures. In this study, fluid-driven displacement across a decimeter-scale laboratory fracture was investigated using the mini-SIMFIP (step rate injection method for fracture in-situ properties) probe, which is a smaller version of the SIMFIP tool (Guglielmi et al., 2014). The mini-SIMFIP probe is able to resolve the full 3D displacement vector of a fracture. The probe was installed in one of two boreholes across a decimeter-scale saw-cut granite fracture. Two pressure step injection tests were conducted under the same isotropic stress conditions. By varying injection between the boreholes, we estimated the aperture profile across the fracture. The results show a consistent pressure-dependent opening as long as steady-state flow was maintained. At a certain pressure step, steady-state conditions were no longer achievable and the fracture opened rapidly. The pressure-opening relationship diverged between the two tests and indicated a homogenization of the aperture profile and an increase in the non-linearity of the flow regime.

1. INTRODUCTION

Developing geothermal reservoirs in the context of enhanced geothermal systems (EGS) requires a comprehensive understanding of hydro-mechanical (HM) couplings in fractured rocks. In-situ injection experiments often lack proper control and sufficient knowledge of fracture properties and the in-situ stress conditions, while laboratory injection tests are typically constrained by small sample sizes, which often suffer from scaling effects and make it challenging to place adequate instrumentation. To address these challenges, we conducted fluid injection experiments in a large-scale laboratory setting, utilizing a novel fiber-optic borehole deformation device, the mini-SIMFIP probe, to investigate the HM coupling of fractures in the laboratory.

The mini-SIMFIP probe is a smaller version of the SIMFIP (step rate injection method for fracture in-situ properties) device, a 3D borehole deformation tool (Guglielmi et al., 2014). At the field scale, the SIMFIP protocol has been effectively used to evaluate stress measurement techniques (Guglielmi et al., 2023; Kakurina et al., 2020) and investigate fault instability related to induced seismicity (Cappa et al., 2019; Guglielmi et al., 2015). In this study, we deployed the mini-SIMFIP probe across an artificial saw-cut fracture in a decimeter-scale granite rock block under true triaxial stress conditions. Under isotropic stress conditions, fracture dislocations were studied during two pressure step tests to assess aperture changes at the injection and monitoring points (8 cm apart), aiming to better understand the HM mechanisms during high-pressure injection tests.

2. METHODS

2.1. Experimental Setup

The decimeter-scale true triaxial testing machine is a modified version of the apparatus used by Deb et al. (2020) and Siebert (2017) for hydraulic fracturing experiments on intact, low-porosity granite. In contrast to their configurations, we employed saw-cut specimens of the same rock type to simulate a pre-existing fracture (see also Ouf et al., 2024). The sample dimensions are 45×30×30 cm, and the fracture runs vertically at a 45° angle to the horizontal axes (Fig. 1). The 45×42 cm

fracture surfaces were polished with 40-grit SiC powder to achieve uniform roughness and stress distribution during compression. Pressure-sensitive film (Fujifilm Pre-Scale LW, range 2.5-10 MPa) was clamped at 5 MPa inside the fracture prior to the injection tests, to visualize the stress distribution along the fracture surface caused by asperity interactions and boundary effects (Fig. 2). Isotropic confining stresses ($\sigma_c = \sigma_1 = \sigma_2 = \sigma_3$) were applied using three sets of oil-filled flatjacks, individually controlled by three hydraulic pumps (type Wille 3 VPC). The pumps recorded the volumetric flow to and from the flatjacks at a sampling rate of 1 Hz. The flatjack pressures, corresponding to the confining stresses, were recorded at 10 Hz using Keller 33X pressure transducers. The flatjacks were clamped between a massive loading frame and steel load plates, which transferred the stresses to the specimen. The load plates were covered with Teflon sheets to minimize friction at the steel-rock interface. All 12 edges of the sample were exposed to the atmosphere. Two boreholes were drilled perpendicular to the fracture plane, extending to the sample edges, to allow fluid injection and placement of the mini-SIMFIP probe. The holes had a diameter of 2 cm and were located 8 cm apart.

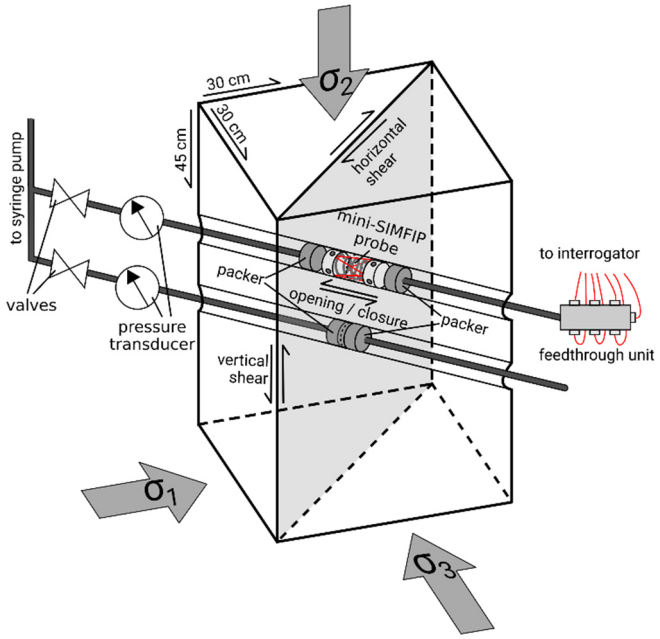

Fig. 1. Scheme of the experimental setup. Boreholes and the mini-SIMFIP probe are not in scale for visualization purposes.

The borehole intervals crossing the fracture were isolated using two separate packers. The spacing between the upper- and lower-hole packers was 120 mm and 4 mm, respectively. Steel capillaries connected the intervals to a continuous flow syringe pump (ISCO 500D). Fluid pressures were recorded at a frequency of 10 Hz by Keller 33X pressure transducers placed outside the sample and the flow rate was recorded by the syringe pump at 1 Hz. Valves allowed switching between the lines or injecting in both boreholes at the same time. Deionized water was used as the injection fluid.

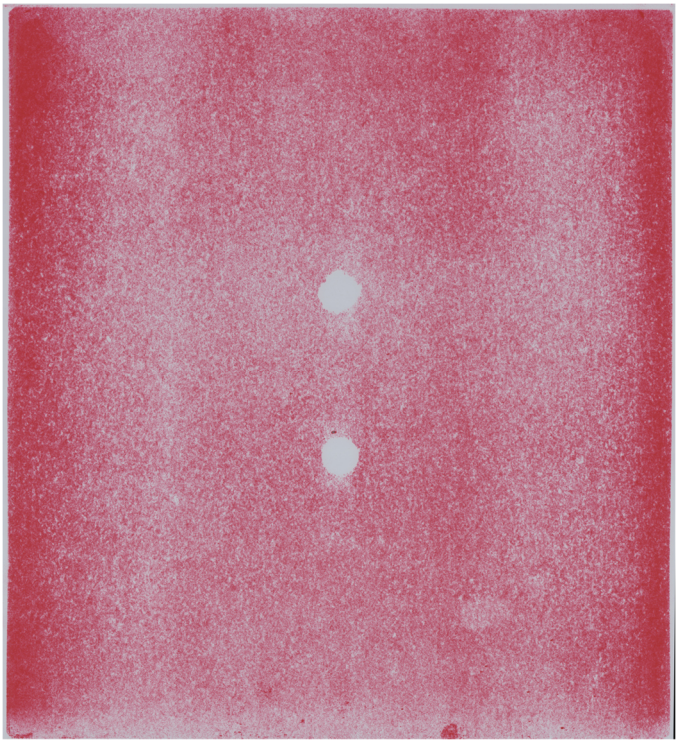

Fig. 2. Pressure-sensitive film, showing the stress distribution on the fracture surface. Higher color intensity indicates higher stress levels and smaller local apertures around the lower borehole compared to the upper one.

2.2. Mini-SIMFIP Probe

A newly developed fiber-optic borehole deformation tool was employed to measure dislocation across the fracture. The mini-SIMFIP probe, a smaller version of the SIMFIP (step rate injection method for fracture in-situ properties) device (Guglielmi et al., 2014), captured the complete 3D displacement of the two rock blocks relative to each other. It has dimensions of 65 mm in length and 19 mm in diameter and was placed in the upper borehole of the sample.

The mini-SIMFIP probe consists of two clamping units connected by a flexible, spring-loaded rod that tensions an array of six fiber optic cables. The clamps were attached to the borehole walls on either side of the fracture. Each fiber optic cable contains a Fiber Bragg Grating (FBG) at the center between the two clamping units. A seventh, untensioned FBG cable was positioned next to the mini-SIMFIP probe in the pressurized interval to account for pressure and temperature effects. All seven fibers were routed through the steel tubing and via a feedthrough unit outside the sample to the interrogator (Luna Hyperion si255). The signals were processed to yield the relative three-dimensional displacements of the clamping units attached to the borehole walls. The feedthrough unit and the relatively long packer interval

resulted in a considerably larger pressurized reservoir in the upper borehole.

2.3. Test Protocol

We conducted two fluid injection tests using the same injection protocol at 3 MPa isotropic confining stress. The main stimulation involved injection in one of the boreholes while the other borehole was sealed. In the first test, we injected into the upper borehole containing the mini-SIMFIP probe to measure the fracture dislocation at the injection point. In the second test, we injected into the lower borehole and measured the fracture dislocation 8 cm apart from the injection point.

The tests started with a saturation phase by injecting into both boreholes with a constant flow rate of 10 ml/min. When a fluid pressure of 0.5 MPa was reached, the pump was switched to pressure control mode and injection was continued in only one borehole. After the saturation phase, the pressure was increased in steps of 0.5 MPa every 120 seconds. This procedure resembles the typical HTPF (hydraulic testing of pre-existing fractures) protocol (Cornet & Valette, 1984), used for field-scale SIMFIP tests as well (Guglielmi et al., 2014, 2020).

3. RESULTS

3.1. Pressure and Flow Rate

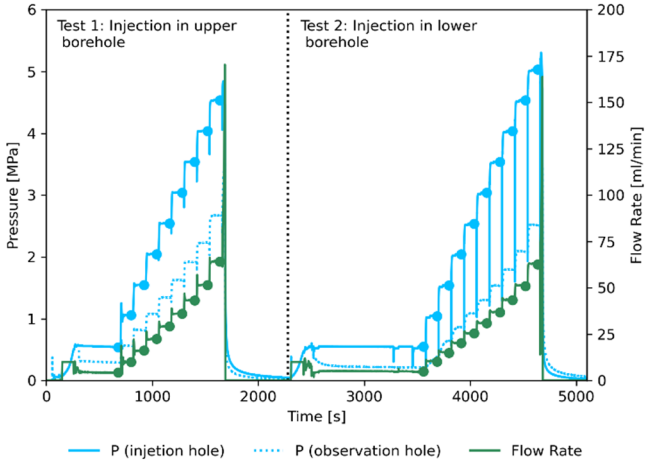

Fig. 3. Flow rate and pressure evolution in the two boreholes during the injection tests. The circles represent the average values of the last 30 seconds of a pressure step.

Fig. 3 illustrates the pressure and flow rate evolution during the two injection experiments. As the pressure at the injection point was increased, the flow rate immediately rose and stabilized within a few seconds. The pressure in the disconnected second borehole also rose and stabilized nearly simultaneously.

In test 1, the flow rate increased sharply when the pressure in the upper borehole was increased from 4.5 MPa to the next step. The target pressure of 5 MPa was not reached as the pressure peaked at 4.8 MPa before slowly declining again. A similar observation was made for test 2, when attempting to elevate the pressure in the lower hole from 5 MPa to 5.5 MPa. To prevent damage to the mini-SIMFIP probe, the injection was stopped (shut-in) approximately 20 seconds after the sharp increase in flow rate began.

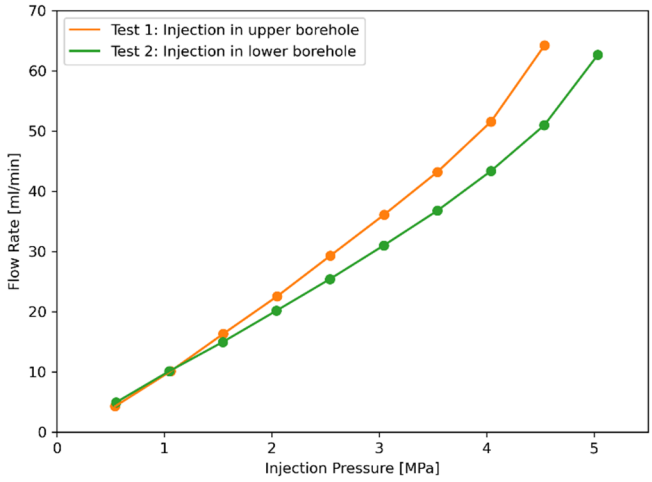

Fig. 4. Steady-state pressure at the injection point and flow rate for each pressure step.

The pressure and flow rate during the last 30 seconds of each step (i.e. under steady-state conditions) were averaged and plotted against each other in Fig. 4, to illustrate the injectivity of the fracture. It is evident, that the injectivity was higher when injecting in the upper borehole (test 1) compared to the lower one (test 2). This could be attributed to the heterogeneity of the fracture surface creating a more permeable area around the upper hole which is consistent with the pressure sensitive film measurements. They indicate slightly higher stresses and therefore more asperity contacts and fewer flow paths around the lower borehole (Fig. 2). We did notice small amounts of water (a few drops accumulated over an hour) leaking from one of the packers in the upper borehole, which could also explain the elevated injectivity. In both tests, the injectivity increased linearly up to 2.5 to 3 MPa, after which it deviated from linearity and became steeper.

3.2. Fracture Displacement

The progressive normal opening and shear displacement measured by the mini-SIMFIP probe closely matched the increase in injection pressure (Fig. 4). Vertically, the fracture moved during the saturation phase around 1µm in one direction, before sliding by 4.5 to 5.5 µm in the opposite direction. The horizontal shear component remained consistent across both tests. During the saturation phase, the fracture experienced a left-lateral slip of 2 to 4 µm. In test 1, this movement progressively increased with each pressure step, ultimately reaching a total offset of 8.5 µm from the initial position. In contrast, sliding in test 2 ceased after a few steps, resulting in a horizontal shear offset of only 2.5 µm.

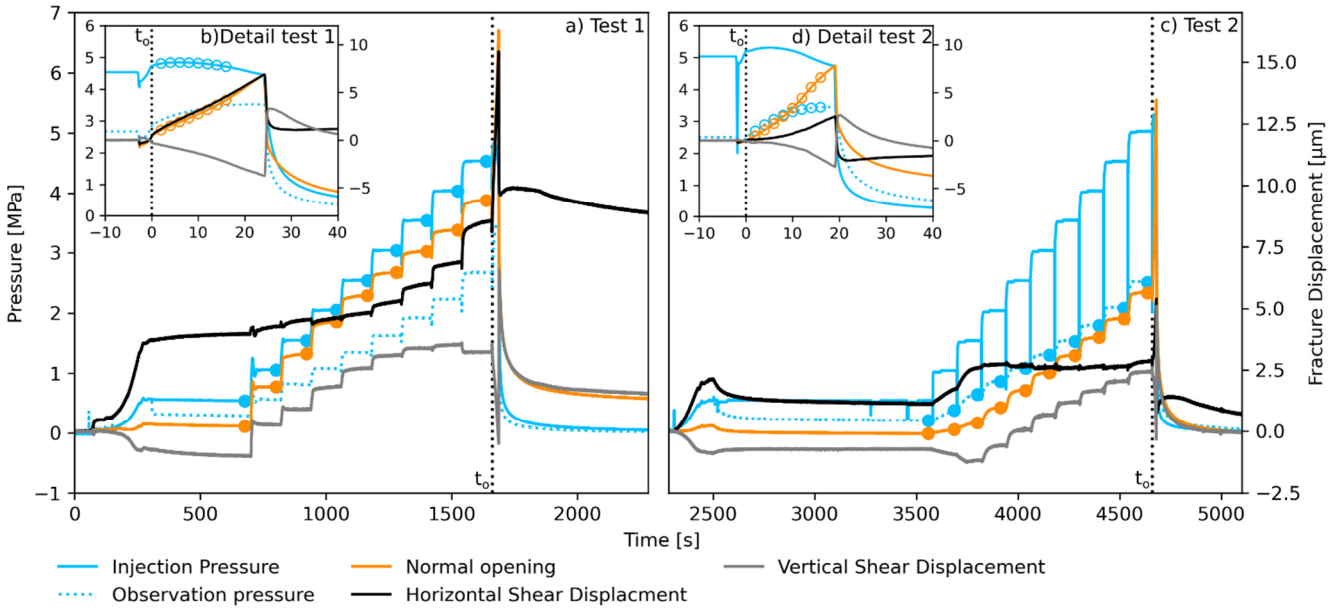

Fig. 5 Pressure evolution in both boreholes and fracture displacement in the upper borehole. Fracture opening is denoted positive. The solid circles in a) and c) represent the average values of the last 30 seconds of a step. t_o indicates the onset of rapid fracture displacement and sharp flow rate increase. The hollow circles in b) and d) represent values every 2 seconds from t_o.

The sharp increase in flow rate following the 4.5 and 5 MPa steps in tests 1 and 2, respectively, coincided with an acceleration in both slip and fracture opening. The onset of this phase is marked as t_0 in Fig. 5a and c, with further details of the time interval around and after t_0 provided in Fig. 5b and d. Following a pressure drop, caused by the syringe pump, the pressure rose again, culminating below the target pressure level. The fracture behavior before t_0 was consistent with earlier pressure steps. However, after t_0, the fracture opened and sheared more rapidly, accompanied by a change in slip direction. Shut-in caused very rapid displacements and a reversal in slip direction. The shear dislocation from t_0 to the end of the tests was largely reversible in both tests. In contrast, there was a considerable permanent offset in the vertical shear component throughout the entire test 1, which was much smaller in test 2.

4. DISCUSSION

4.1. Occurrence of Shear Displacement

Since all flatjacks maintained the same pressure, no shear stress on the fracture and therefore no shear displacement would be expected. However, the inhomogeneous distribution of friction, stress, and fluid pressure on the fracture surface could have contributed to fracture-parallel slip. The significant shear offset observed in the first test is also reflected in the volume changes of the individual confining pumps. We attribute these dislocations to residual stresses from the loading and unloading phases before the injection tests, which were largely relieved after test 1.

Fracture Opening Behavior

In HTPF tests, the deviation from linearity in the P-Q plot (Fig. 4) is often referred to as the jacking pressure and is used to estimate the normal stress on fractures. However, the jacking pressure may underestimate the normal stress due to pressure diffusion in the fracture plane (Krietsch, 2019; Rutqvist & Stephansson, 1996) or overestimate the normal stress due to channeling effects (Cornet et al., 2003). While the jacking pressure in the two tests presented is around 2.5 to 3 MPa and corresponds quite well to the normal stress, previous experiments in a similar setup (Osten et al., 2023) have shown differences between the jacking pressure and the fracture normal stress. Furthermore, the deviation from linearity is gradual and not straightforward to pick.

We observed significant fracture opening at the injection and the observation point from the start of injection as a function of the local fluid pressure (Fig. 6). While mechanical fracture opening during the first steps of a pressure step test is often considered neglectable (Krietsch, 2019), conceptual models (Ouf et al., 2024; Rutqvist & Stephansson, 1996) and laboratory and in-situ experiments at comparable fracture normal stresses (Cappa et al., 2019) indicate fracture opening from almost the beginning of injection.

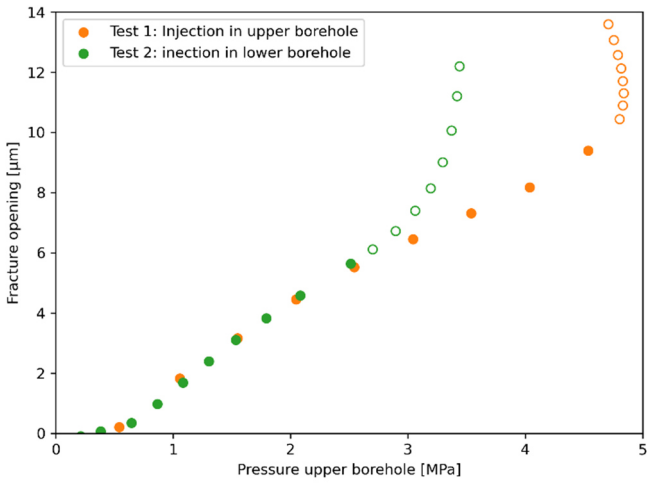

Fig. 6. Local pressure vs. fracture opening. The data points were taken from Fig 5. The solid circles represent steady-state values and the hollow circles were taken every 2 seconds from t_0.

4.2. Fracture Aperture Distribution

To compare the relationship between pressure and opening at the injection point and the remote monitoring borehole, the results from test 1 and test 2 were combined. Before t_0, we averaged the opening and corresponding fluid pressure during the last 30 seconds of each step, which represent steady-state flow conditions. These values are shown as solid circles in Figs. 5 and 6. After the sharp increase in flow rate at t_0, it was not possible to extract further steady-state values. Therefore, pressure and opening values were picked every 2 seconds from t_0 onward, as indicated by the hollow circles in Figs. 5 and 6.

During the steady state phase, the relation between pressure and fracture opening was the same at the injection point and in the remote monitoring borehole (Fig. 6). However, after t_0 the flow rate sharply increased and the fracture opened rapidly at both locations. At the injection point, the opening even continued after the pressure slightly declined. At the remote observation point, the pressure-opening relation deviated from the steady-state behavior observed at the injection point for the respective pressures. These findings suggest a strong increase in fluid volume inside the fracture.

Fig. 7 illustrates the aperture distribution along the fracture. In the initial stage of the tests, as steady-state flow was reached, the fracture opening gradient between the two boreholes became slightly steeper with increasing fluid pressure. We assume that there was no opening at the zero-pressure fracture boundaries during that stage. When the rapid opening started at t_0 the displacement was decoupled from the local fluid pressures. As the opening progressed, the aperture gradient between the two boreholes decreased. This homogenization of the aperture profile is attributed to an increase in the non-linearity of the flow regime, which no longer maintains steady-state conditions. The opening behavior near the fracture boundaries remains uncertain during this phase. While we still assume zero-pressure fracture boundaries, the apparent decoupling of pressure and opening suggests that a change in aperture, potentially indicating the lift-off of the entire fracture, cannot be ruled out.

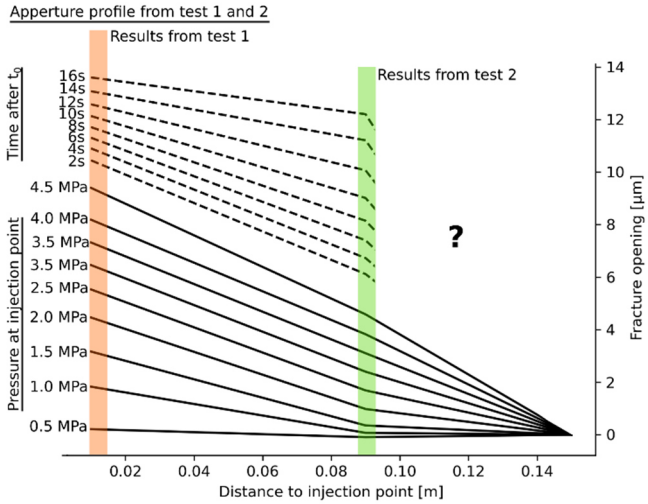

Fig. 7. Changes of the aperture profile from combining the results of the two injection tests. The datapoints correspond to the circles in Fig. 5.

5. CONCLUSION AND OUTLOOK

A new laboratory deformation tool, the mini-SIMFIP probe was successfully deployed in a decimeter-scale laboratory setup. By conducting two pressure step injection tests under the same isotropic stress conditions in different boreholes, we were able to analyze and compare fluid-driven fracture displacement, with a particular focus on normal opening across the fracture.

The results suggest that the pressure-opening relationship was consistent both at the injection point and in a remote monitoring borehole as long as steady-state flow was maintained. However, once a certain pressure step was reached, steady-state flow could no longer be sustained, and the fracture opened rapidly. The relationship between fluid pressure and fracture opening diverged between the two displacement measurement points, indicating a homogenization of the aperture profile and an increase in the non-linearity of the flow regime.

Because the results presented combine the findings of two separate injection tests under the same stress conditions, it would be beneficial to measure fracture displacement at various locations during a single test. Furthermore, as the experimental setup allows for modification of stress magnitude and anisotropy, we plan to conduct additional fluid injection tests to explore not only local opening and closure but also fracture-parallel slip and fault reactivation under different stress conditions.

6. REFERENCES

1. Cappa, F., Scuderi, M. M., Collettini, C., Guglielmi, Y., & Avouac, J.-P. (2019). Stabilization of fault slip by fluid injection in the laboratory and in situ. Science Advances, 5(3). https://doi.org/10.1126/sciadv.aau4065
2. Cornet, F. H., Li, L., Hulin, J.-P., Ippolito, I., & Kurowski, P. (2003). The hydromechanical behaviour of a fracture: An in situ experimental case study. International Journal of Rock Mechanics and Mining Sciences, 40(7–8), 1257–1270. https://doi.org/10.1016/S1365-1609(03)00120-5
3. Cornet, F. H., & Valette, B. (1984). In situ stress determination from hydraulic injection test data. Journal of Geophysical Research: Solid Earth, 89(B13), 11527–11537. https://doi.org/10.1029/JB089iB13p11527
4. Deb, P., Düber, S., Guarnieri Calo' Carducci, C., & Clauser, C. (2020). Laboratory-scale hydraulic fracturing dataset for benchmarking of enhanced geothermal system simulation tools. Scientific Data, 7(1), 220. https://doi.org/10.1038/s41597-020-0564-x
5. Guglielmi, Y., Cappa, F., Avouac, J.-P., Henry, P., & Elsworth, D. (2015). Seismicity triggered by fluid injection–induced aseismic slip. Science, 348(6240), 1224–1226. https://doi.org/10.1126/science.aab0476
6. Guglielmi, Y., Cappa, F., Lançon, H., Janowczyk, J. B., Rutqvist, J., Tsang, C. F., & Wang, J. S. Y. (2014). ISRM Suggested Method for Step-Rate Injection Method for Fracture In-Situ Properties (SIMFIP): Using a 3-Components Borehole Deformation Sensor. Rock Mechanics and Rock Engineering, 47(1), 303–311. https://doi.org/10.1007/s00603-013-0517-1
7. Guglielmi, Y., McClure, M., Burghardt, J., Morris, J. P., Doe, T., Fu, P., Knox, H., Vermeul, V., Kneafsey, T., The EGS Collab Team (2023). Using in-situ strain measurements to evaluate the accuracy of stress estimation procedures from fracture injection/shut-in tests. International Journal of Rock Mechanics and Mining Sciences, 170, 105521. https://doi.org/10.1016/j.ijrmms.2023.105521
8. Guglielmi, Y., Nussbaum, C., Rutqvist, J., Cappa, F., Jeanne, P., & Birkholzer, J. (2020). Estimating perturbed stress from 3-D borehole displacements induced by fluid injection in fractured or faulted shales. Geophysical Journal International, 221(3), 1684–1695. https://doi.org/10.1093/gji/ggaa103
9. Kakurina, M., Guglielmi, Y., Nussbaum, C., & Valley, B. (2020). In Situ Direct Displacement Information on Fault Reactivation During Fluid Injection. Rock Mechanics and Rock Engineering, 53(10), 4313–4328. https://doi.org/10.1007/s00603-020-02160-w
10. Krietsch, H. (2019). Hydro-Mechanical Responses of a Fractured Rock Mass during Decameter-Scale Hydraulic Stimulation Experiments [Doctoral Thesis, ETH Zurich]. https://doi.org/10.3929/ethz-b-000372209
11. Osten, J., Cadmus, A., Jalali, M., Fuentes, R., & Amman, F. (2023). Decimeter-scale hydraulic testing of pre-existing Fractures (HTPF) under anisotropic stress conditions. Part 2: Test procedure and results [Poster]. GeoBerlin 2023. 10.48380/0n83-sq10
12. Ouf, J., Osten, J., Luo, W., Khaledi, K., Jalali, M., Vardon, P. J., & Amann, F. (2024). Experimental and numerical analysis of injection-induced permeability changes in pre-existing fractures. Geomechanics for Energy and the Environment, 39, 100576. https://doi.org/10.1016/j.gete.2024.100576
13. Rutqvist, J., & Stephansson, O. (1996). A cyclic hydraulic jacking test to determine the in situ stress normal to a fracture. International Journal of Rock Mechanics and Mining Sciences & Geomechanics Abstracts, 33(7), 695–711. https://doi.org/10.1016/0148-9062(96)00013-7
14. Siebert, P. (2017). Laborversuche zur hydraulischen Risserzeugung in dreiaxial belasteten Granitquadern [Doctoral Thesis, RWTH Aachen University].